JOURNAL OF MATERIALS SCIENCE 26 (1991) 2997–3003

Surface tension measurements of liquid metals by the oscillating drop technique

I. EGRY
Institute for Space Simulation, German Aerospace Research Establishment, 5000 Köln-90, FRG

An improved method for measuring the surface tension of liquid metals is proposed. Surface oscillations of an electromagnetically levitated liquid metal droplet are observed by a video camera and digital image processing is used to evaluate the spectrum of oscillations. A discussion of the theoretical background and a description of the experimental apparatus are presented. In addition, preliminary results on an FeNi sample, and an outlook for future experiments, including the measurement of viscosity, are given.

1. Introduction

The surface tension of liquid metals is a technologically important and scientifically interesting parameter. It dominates many metallurgical processes, such as casting, welding and melt spinning. A first principles calculation of the surface tension would require a microscopic model of the liquid state, including density and free-energy profiles at the surface. Such theories exist at present only for very simple systems [1]. Experimentally, there is a large scatter between available data. This can be attributed to contamination of the surface, in particular by oxygen. Earlier work is reviewed by Allen [2], while more recently a review for iron and its binary alloys has been given by Keene [3].

Conventionally, surface tension measurements are carried out using the sessile-drop or pendant-drop techniques [4]; these techniques determine the non-spherical equilibrium shapes of drops due to surface tension and gravity. The inherent difficulties of this method are discussed by Sangiorgi *et al.* [5]. An alternative approach to surface tension measurements is the oscillating drop technique using electromagnetic levitation. This method avoids any contact with a crucible and thus reduces not only systematic errors due to surface contamination but also allows deep undercooling of the liquid metal [6]. The restoring force for surface oscillations is the surface tension, which therefore can be related to the frequency of the oscillations [7].

Electromagnetic levitation can be improved further by utilizing the microgravity environment on board an orbiting spacecraft. The residual acceleration is of the order of $\approx 10^{-3} g_0$–$10^{-5} g_0$ where $g_0 = 9.81\ \mathrm{m\,s^{-2}}$. Accordingly, much lower electromagnetic fields are necessary. This has essentially two consequences: first, the induced currents in the sample are reduced, leading to less power dissipation and weaker stirring effects; second, the magnetic "pressure" on the sample surface is reduced, and third, the sample remains essentially spherical. The magnetic pressure leads to an apparent increase in the surface tension, which is usually neglected and a spherical shape greatly facilitates the oscillation analysis. Based on these considerations, we have proposed a microgravity experiment for measuring surface tension and viscosity of undercooled metallic melts [8].

Terrestrial measurements using the oscillating drop technique have been first carried out by Fraser *et al.* [9] and, more recently, by Schade *et al.* [10] and Keene *et al.* [11]. Fraser *et al.* used high-speed cinematography for recording the surface oscillations, while the latter used a photodetector which records the incoming (oscillating) light intensity. Upon analogue/digital-conversion, the signal can be analysed by fast Fourier transformation (FFT); this facilitates the experimental evaluation considerably, compared to the tedious manual and visual analysis of the photographs of Fraser *et al.* However, there is a shortcoming in this technique: because the intensity is an integrated signal, information is lost about the actual type of oscillation. This becomes a serious problem, if, as is usually the case, there is more than one oscillation frequency. In order to attribute the measured frequencies to the corresponding normal modes, some information about the actual shape of the oscillating drop is required. Slits in front of the detector act as a filter for certain oscillatory modes and can be used to suppress their contribution to the signal.

In this paper we present another solution to this problem, which in a sense can be regarded as the combination of the two above mentioned methods: we record the oscillations by a suitable video camera and use subsequent digital image processing. The recorded frames contain the full two-dimensional image from which the desired information can be extracted. Liggieri and Passerone [12] have also applied automatic digital image processing routines for measuring the surface tension of liquid metals. They employed the sessile drop technique and analyse static images. In their approach, the spatial resolution of the video camera is the limiting factor, whereas for the

0022–2461/91 $03.00 + .12

oscillating drop technique the temporal resolution is crucial.

We were able to apply our image processing scheme to video images which were taken during preliminary performance tests of an electromagnetic microgravity levitation facility on board a KC-135 aircraft. Although these tests were not intended for scientific experiments and, accordingly, the conditions were far from optimal, the analysis yielded surprisingly good results for the surface tension of an FeNi sample.

2. Theory

2.1. Levitation

An inhomogeneous, alternating electromagnetic field has two effects on a conducting, diamagnetic body: firstly, it induces eddy currents within the material, which, due to ohmic losses, eventually heat up the sample (inductive heating), and secondly, it exerts a force on the body pushing it towards regions of lower field strength (Lorentz force). The latter effect can be used to compensate the gravitational force acting on the body. This is the principle of levitation melting, as first formulated by Okress *et al.* [13].

More explicitly, the power, P, absorbed by a sample of volume, V, averaged over a time, τ, is given by

$$P = \frac{1}{\tau}\int_0^{\tau}\int_V \frac{j_{\mathrm{ind}}^2}{\tilde{\sigma}}\,\mathrm{d}V\,\mathrm{d}t \qquad (1)$$

where $\tilde{\sigma}$ is the electrical conductivity of the sample and j_{ind} the induced current.

For a homogeneous magnetic field, $\boldsymbol{B}$, an approximate analytical expression can be given for a spherical sample of radius, R,

$$P = \frac{3\pi R}{\tilde{\sigma}\mu_0^2} H(q)\boldsymbol{B}^2 \qquad (2)$$

where

$$H(q) = q\frac{\sin\mathrm{h}(2q) + \sin(2q)}{\cos\mathrm{h}(2q) - \cos(2q)} - 1 \qquad q = R/\delta \qquad (3)$$

The quantity of interest in this expression is δ, the skin depth. It is given by

$$\delta = \left(\frac{2}{\omega\tilde{\sigma}\mu_0}\right)^{1/2} \qquad (4)$$

where ω is the angular frequency of the electromagnetic field. For frequencies in the megahertz range, the skin depth is ≈ 0.1 mm for most metals. The heating efficiency has a maximum for $q \approx 2$ and can, in principle, be optimized for a given conductivity by selecting the appropriate frequency. A more detailed treatment can be found in [14].

The time-averaged force acting on a conducting sample can be calculated from

$$\boldsymbol{F} = \frac{1}{\tau}\int_0^{\tau}\int_V \boldsymbol{j}\times\boldsymbol{B}\,\mathrm{d}V\,\mathrm{d}t \qquad (5)$$

For a weakly non-homogeneous magnetic field, the following expression can be derived

$$\boldsymbol{F} = -\frac{\pi R^3}{\mu_0} G(q)\nabla B^2 \qquad (6)$$

where:

$$G(q) = 1 - \frac{3}{2q}\frac{\sin\mathrm{h}(2q) - \sin(2q)}{\cos\mathrm{h}(2q) - \cos(2q)} \qquad (7)$$

As can be seen, an inhomogeneous field pushes the sample into regions of low magnetic field strength. The force increases with increasing conductivity.

If a quadrupole field as shown in Fig. 1 is applied, it compensates not only gravitational forces, but also stabilizes the sample against vertical and lateral displacements from its equilibrium position. In first order, the equation of motion for the centre of mass of the sample is that of an harmonic oscillator with a frequency

$$\nu = \frac{1}{2\pi}\left(\frac{k}{M}\right)^{1/2} \qquad k \sim \nabla\boldsymbol{F} \qquad (8)$$

where M is the mass of the sample. For metal spheres with $R \approx 5$ mm, ν is usually in the order of 3–5 Hz.

Forces acting on a liquid sample inevitably deform its shape. This is true for both the gravitational and the electromagnetic force. Calculations of the equilibrium shape are given by Gagnoud [15] and Cummings and Blackburn [16]. As we will see in the next section, any non-sphericity introduces complications into the spectrum of oscillations and should therefore be avoided. As mentioned before, this is one reason for carrying out such experiments under microgravity conditions.

2.2. Drop oscillations

Surface tension and viscosity can be measured by exciting surface oscillations of a levitated drop. The frequency, ω, of the oscillations is related to the surface tension, σ, while the damping, γ, yields the viscosity, η. The theory of oscillations of a liquid drop is a classical problem in hydrodynamics and has been treated to several degrees of sophistication.

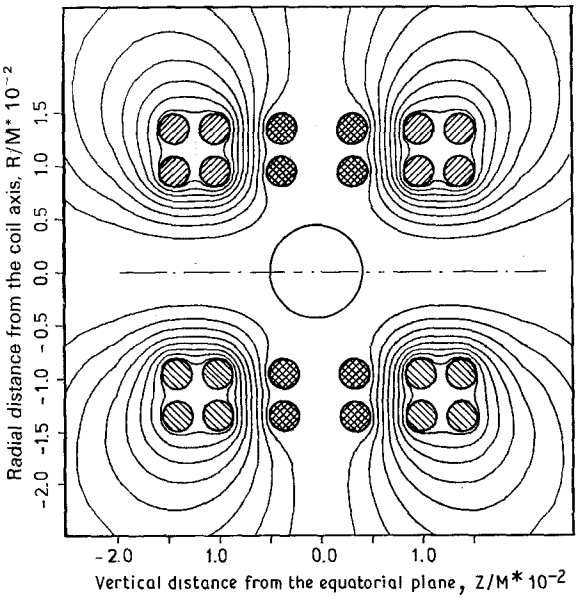

Figure 1 The quadrupole field used to position and stabilize a metallic drop. Also shown are the heating and positioning coils.

The radius of a spherical droplet [7] undergoes oscillations of the form

$$R_l \sim \cos(\omega_l t)\mathrm{e}^{-\gamma_l t} P_l(\cos\theta) \quad (9)$$

where t is the time and θ is the angle with respect to the symmetry axis, l is the index of the normal mode and P_l is a Legendre polynomial.

In the linearized theory, frequency, ω_l, and damping, γ_l, are given by

$$\omega_l = [l(l-1)(l+2)\sigma/(\rho R_0^3)]^{1/2} \quad (10)$$

$$\gamma_l = (l-1)(2l+1)\eta/(\rho R_0^2) \quad (11)$$

where R_0 is the unperturbed radius and ρ is the density of the sphere. The fundamental mode is $l = 2$.

For this mode, Cummings and Blackburn [16] have calculated the effect of asphericity, gravity, magnetic field and sample rotation on the frequency for an inviscid drop. The main result of their calculation is that the frequency of the fundamental $l = 2$-mode is split into upto five sidebands, or, to put it in quantum-mechanical terms, the five-fold degeneracy of $l = 2$ is lifted. This is due to the fact that Equation 9 is not the most general solution for aspherical drops. Allowing for azimuthal dependence of the radius, it is given by spherical harmonics

$$R_{l,m} \sim \cos(\omega_{l,m} t)\mathrm{e}^{-\gamma_{l,m} t} P_l^m(\cos\theta)\cos[m(\varphi - \varphi_0)] \quad (12)$$

where φ_0 is an (arbitrary) symmetry direction, $|m| \leqslant l$ and P_l^m is an associated Legendre function, related to P_l by

$$P_l^m(x) = (-1)^m(1-x^2)^{m/2}\frac{\mathrm{d}^m}{\mathrm{d}x^m}P_l(x) \quad (13)$$

For reference, we list below the P_2^m associated Legendre functions

$$\begin{aligned} P_2^0(\cos\theta) &= \tfrac{1}{4}(3\cos 2\theta + 1) \\ P_2^1(\cos\theta) &= -\tfrac{3}{2}\sin 2\theta \\ P_2^2(\cos\theta) &= \tfrac{3}{2}(1-\cos 2\theta) \end{aligned} \quad (14)$$

For a non-rotating spherical droplet, the $l = 2$ modes are five-fold degenerate

$$\omega_{2,m} = \omega_2 \quad (15)$$

If the equilibrium shape is no longer spherical but still axisymmetric and the sample does not rotate, the frequencies depend on $|m|$ only, and one expects three peaks in the spectrum, namely $m = 0, \pm 1, \pm 2$. A rotating and/or not axisymmetric sample will exhibit all five peaks.

In addition to frequency splitting, the frequencies are also shifted with respect to Equation 10. The shift is proportional to the translational and rotational frequencies of the sample and its asphericity. According to Cummings and Blackburn [16], rotation influences only $m \neq 0$ modes

$$\omega_{l,m}^{\mathrm{r}} = \omega_{l,m}^0 + \frac{m}{2}\Omega \quad (16)$$

where Ω is the rotational frequency around the z-axis. Translational oscillations affect all frequencies. However, Cummings and Blackburn [16] have derived the following sum rule

$$\omega_2^2 = \frac{1}{5}\sum_{m=-2}^{+2}\omega_{2,m}^2 - 2\omega_{\mathrm{t}}^2 \quad (17)$$

where ω_{t} is the translational frequency.

2.3. Image processing

The oscillations can be detected as variations in the shape of the sample. The video camera produces a two-dimensional image of the sample which is given by the projection of the sample on to a plane normal to the viewing direction.

It is sufficient to assume that the sample is oscillating at a single frequency. Owing to the orthogonality of the Legendre functions, contributions from different modes can be superimposed linearly.

For a top view, i.e. looking along the z-axis, the circumference of the image at a time, t, is given by

$$\tilde{R}_{l,m}^{\mathrm{top}}(\varphi, t) = \max_{\theta}\{R_0[1 + \varepsilon(t)R_{l,m}(\theta, \varphi)]\sin\theta\} \quad (18)$$

where φ is the viewing direction and

$$\varepsilon(t) = \varepsilon_0\cos(\omega_{l,m} t)\mathrm{e}^{-\gamma_{l,m} t} \quad (19)$$

is the time-dependent amplitude of the oscillation.

For small $\varepsilon_0 \ll 1$ (a condition that must be satisfied anyway in a linearized theory), the above definition yields the equatorial cross-section of the sample

$$\tilde{R}_{l,m}^{\mathrm{top}}(\varphi, t) = R_0\left[1 + \varepsilon(t)R_{l,m}\left(\frac{\pi}{2}, \varphi\right)\right] \quad (20)$$

which for $m = 0$ is a circle. Note that $P_2^1[\cos(\pi/2)] = 0$.

For a side view, say along the x-axis, one obtains similarly

$$\tilde{R}_{l,m}^{\mathrm{side}}(\theta, t) = \max_{\varphi}\{R_0[1 + \varepsilon(t) R_{l,m}(\theta, \varphi - \varphi_0)]\sin\varphi\} \quad (21)$$

Here, φ_0 is not necessarily the viewing direction. As before, one obtains for small $\varepsilon \ll 1$ the cross-section

$$\tilde{R}_{l,m}^{\mathrm{side}}(\theta, t) = R_0\left[1 + \varepsilon(t)R_{l,m}\left(\theta, \frac{\pi}{2} - \varphi_0\right)\right] \quad (22)$$

Deriving surface tension values from measured frequency spectra with several peaks requires the identification of each of the peaks with their corresponding labels (l, m). This can be done by analysing the shape of the oscillating drop. The $l = 2$ modes are shown in Figs 2–4 when viewed from the side. For sake of clarity, a large $\varepsilon = \pm 0.2$ has been chosen, which is outside the scope of linear theory. It is convenient to create binary images choosing a suitable threshold. In this case the sample will be displayed white, whereas the remainder of the picture will be black. This step eliminates the effect of temperature on the signal and suppresses any unwanted reflections. Once the binary image has been obtained, there exist a number of

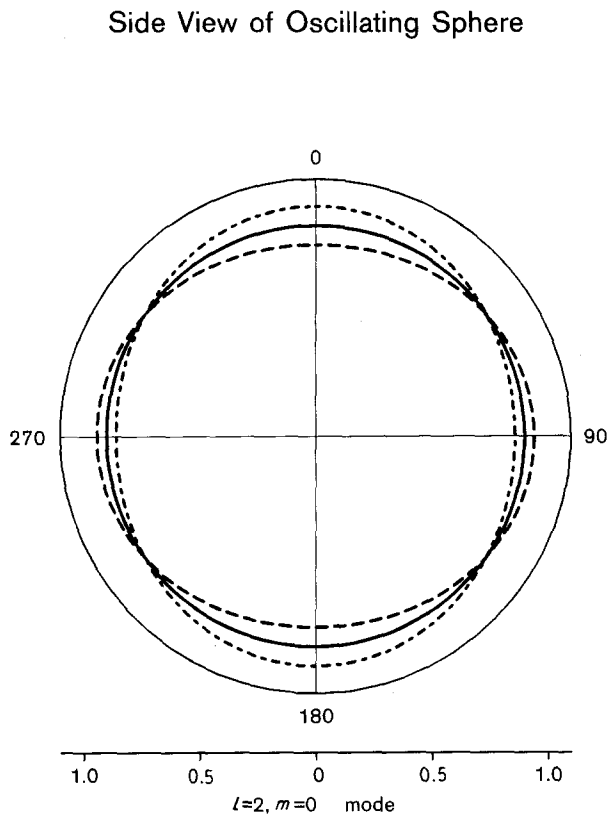

Figure 2 $l = 2$, $m = 0$ oscillation of a sphere, side view for $\varepsilon = 0.2$, 0.0, -0.2.

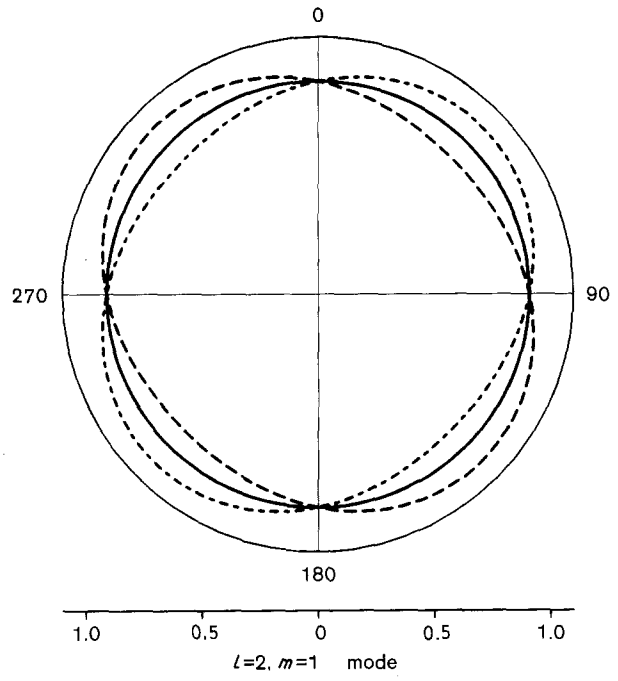

Figure 3 $l = 2$, $m = 1$ oscillation of a sphere, side view for $\varepsilon = 0.2$, 0.0, -0.2.

methods to extract information from it. One way is to determine directly the radius at a suitably chosen fixed angle, θ_0. According to Equation 12, the temporal change of this quantity directly yields frequency and damping. This method mimics the use of slits in the conventional measurements [10]. By choosing the appropriate angle, one can suppress signals from

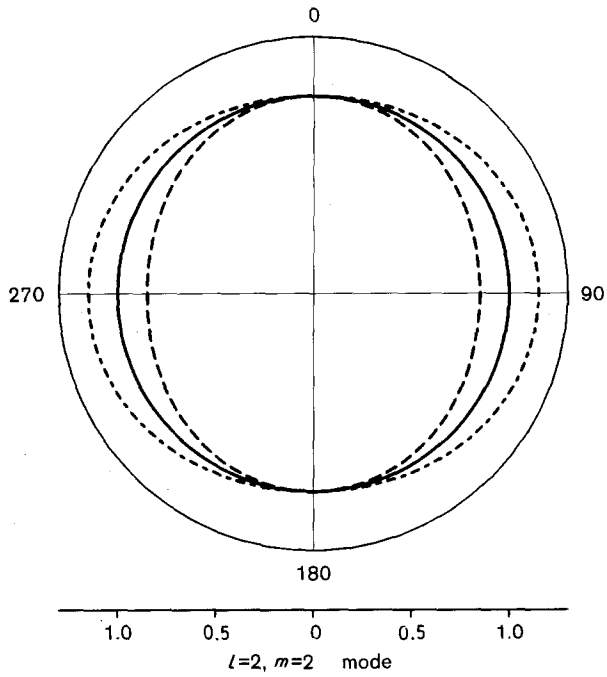

Figure 4 $l = 2$, $m = 2$ oscillation of a sphere, side view for $\varepsilon = 0.2$, 0.0, -0.2.

certain modes. For example

$$P_2\,[\cos(54.7°)] \;=\; 0 \tag{23}$$

while $P_2^m \neq 0$ for $m = 1, 2$. The problem with this approach is, that the centre of mass of the sample must be known; this is the point from which the radius vector is to be drawn. If the sample undergoes translational oscillations, this point is not fixed and must be determined for each frame.

Another possibility is to use the total number of white pixels, i.e. the area of the cross-section, as the signal. For a side view the cross-section, Q, is given by

$$Q_{l,m}^{\text{side}}(t) \;=\; 2\int_0^{\pi} \mathrm{d}\theta \int_0^{\tilde{R}_{l,m}^{\text{side}}} \mathrm{d}r\, r \tag{24}$$

which yields upon insertion of Equation 22 and linearization

$$Q_{l,m}^{\text{side}}(t) \;=\; \pi R_0^2 \left[1 \;+\; \varepsilon(t)\frac{2}{\pi}\int_0^{\pi} \mathrm{d}\theta\, P_l^m(\cos\theta)\right] \tag{25}$$

For odd l or m the integral vanishes, which again constitutes a selection rule. This analysis is insensitive to translations of the sample, as long as the whole cross-section remains visible.

When viewing from the top, one obtains

$$\begin{aligned} Q_{l,m}^{\text{top}}(t) &= \int_0^{2\pi} \mathrm{d}\varphi \int_0^{\tilde{R}_{l,m}} \mathrm{d}r\, r \\ &= \pi R_0^2\,[1 \;+\; 2\varepsilon(t) P_l^m(0)\delta_{m,0}] \end{aligned} \tag{26}$$

This last expression again implies a selection rule.

If necessary, one can use a more general signal $S(t)$ by defining a filter function $F(\theta, r)$

$$S(t) \;=\; 2\int_0^{\pi} \mathrm{d}\theta \int_0^{\tilde{R}_{l,m}} \mathrm{d}r\, r\, F(\theta, r) \tag{27}$$

In this latter definition, the cross-section is contained

as the special case $F = 1$. It is the strength of image processing that one is free to choose any suitable F.

The frequencies $\omega_{l,m}$ can be determined by Fourier transforming the signal. To obtain the damping, one may use the halfwidth, $\Delta\nu$, of the frequency peak according to the relation

$$\gamma = \pi\Delta\nu \tag{28}$$

where $\Delta\nu$ is the width of the peak at $1/2^{1/2}$ maximum height. This method is only viable if the peaks are well resolved and the measuring time, $\Delta\tau$, is much larger than the damping time, due to the uncertainty relation inherent in Fourier transformation

$$\Delta\nu_{\min}\,\Delta\tau \approx 1 \tag{29}$$

Hence, all peaks have a minimum linewidth of the order $1/\Delta\tau$. Alternatively, one may obtain at least the smallest damping from the time signal directly. Discarding the initial transient phase, where all modes with strong damping die out, the logarithmic decrement during one period T_0 yields the damping directly

$$\frac{\ln S(t + T_0) - \ln S(t)}{T_0} = -\gamma \tag{30}$$

For practical purposes, it is convenient to square the signal before taking the logarithm.

3. Experiments

3.1. Levitation

The experiments were carried out using the development model of the TEMPUS facility, an electromagnetic levitation facility designed to operate under microgravity conditions. It is shown schematically in Fig. 5. TEMPUS uses a two-coil, two-frequency concept which allows variation of the heating (dipole) field and the positioning (quadrupole) field independently.

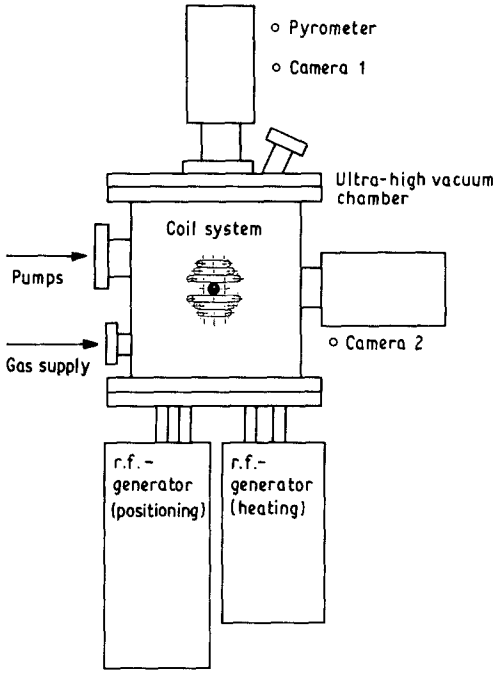

Figure 5 Schematic view of TEMPUS, showing the camera positions.

The coil systems are optimized for maximum efficiency: most metals can be positioned against $10^{-2}\,g_0$ and heated up to 2500 °C with only 1.5 kW. By switching off the heating field, the power input into the sample can be minimized to ≈ 10 W, thereby allowing undercooling without forced gas cooling of the sample. In addition, a short voltage pulse through the heating coil can be used to excite the surface oscillations.

TEMPUS is equipped with a two-colour pyrometer measuring between 300 and 2500 °C with a sampling rate of 1 MHz. Two video cameras (standard CCIR monochrome) offer top and side view. The facility can operate under inert purified gas atmosphere (Ar, He) and ultra-high vacuum (10^{-9} mbar). Due to the coil geometry, spherical samples with radius $R_0 \leqslant 0.5$ cm can be processed.

TEMPUS cannot levitate against 1 g. Therefore, it had to be tested during parabolic flights on a KC-135 airplane. Each parabola provides about 10 s of $10^{-2}\,g_0$. The original intention was to test the positioning capabilities of TEMPUS only. It turned out, however, that the time was sufficient to position and melt the sample, and to excite surface oscillations. An $Fe_{75}Ni_{25}$ sample with a melting point of $T_m = 1550$ °C and 4.2 g mass was used and processed in an He atmosphere.

3.2. Image processing

The images were recorded on a VHS video recorder. Standard CCIR–TV uses 25 full frames per second, each containing 590×600 pixels. One full frame consists of two half frames (295×600). Using all half frames, a sample rate of 50 Hz is achieved. According to the Nyquist sampling condition [17], the maximum frequency that can be resolved is therefore 25 Hz. The frequency of the $l = 2$ mode lies in the region of 20 Hz and cannot be detected on full frames. It is therefore essential to use video recorders which display all half frames. We have used a Panasonic AG 7330 EG which has half frame by half frame backward and forward scanning capability. In the future, a modified video camera with a frame rate of up to 500 Hz will be used.

For image acquisition and image processing, the Interactive Data Language (IDL) software of RSI® was employed. In order to reduce storage requirements, only that section of the images was digitized and stored which contains the essential information, i.e. the sample. Nevertheless, there is a considerable amount of data to be stored, for a 10 s sequence approximately 100 Mbyte.

Owing to the coil and sample holder geometry, the limb of the sample was not entirely visible from the top, and the poles were not visible from the side. For frequency analysis, we used only side views of the sample and evaluated either the width of the sample at different heights, or the total visible area of the sample. The best results were obtained using the area.

For any choice of filter function, F (Equation 27), one obtains a single real number for each frame, thereby reducing the amount of data by a factor of

10^5. The final result of image processing is therefore a real-valued vector of length $L = f\Delta\tau \approx 500$, where f is the sampling rate and $\Delta\tau$ is the measuring time. This time signal is then Fourier transformed to obtain the linear frequency spectrum.

4. Results and discussion

4.1. Parabolic flight

We used Equation 25 to obtain the time signal. The first 4 s are shown in Fig. 6. In the first 2 s of the experiment, the sample is solid and shows no oscillation. It is then heated above its melting point up to 1580 °C and oscillations are externally excited at $t \approx 2.5$ s. Solidification occurs at $t \approx 8$ s.

For the frequency analysis, only that part of the signal was used, which is free from transient disturbances. The Fourier transform of the time interval from $t = 3.8$–5.8 s is shown in Fig. 7. In addition to some low-frequency peaks, which can be attributed to translational motion of the sample, it shows a sharp peak at $\nu = 17.8$ Hz. We attribute this peak to the ($l = 2$, $m = 0$) mode. This is supported by visual inspection of the video recordings. It should also be mentioned that the Fourier transform of the first 2 s (solid sample) does show the same low-frequency peaks, but none at high frequencies. This confirms that those peaks are not an artefact of the analysis, but a genuine reflection of the oscillations of the liquid sample.

Inserting the measured frequency into Equation 10 which for $l = 2$ reads

$$\sigma = \tfrac{3}{8}\pi M\nu^2 \tag{31}$$

where M is the mass of the sample, which in our case was $M = 4.2$ g, we obtain $\sigma = 1.6\ \mathrm{N\,m^{-1}}$. Values reported in the literature [3], are in the range 1.5–1:8 $\mathrm{N\,m^{-1}}$. The relatively low value obtained here can be attributed to contamination of the sample surface by oxygen. In fact, a post-flight analysis of the sample showed an oxygen content of about 100 p.p.m.

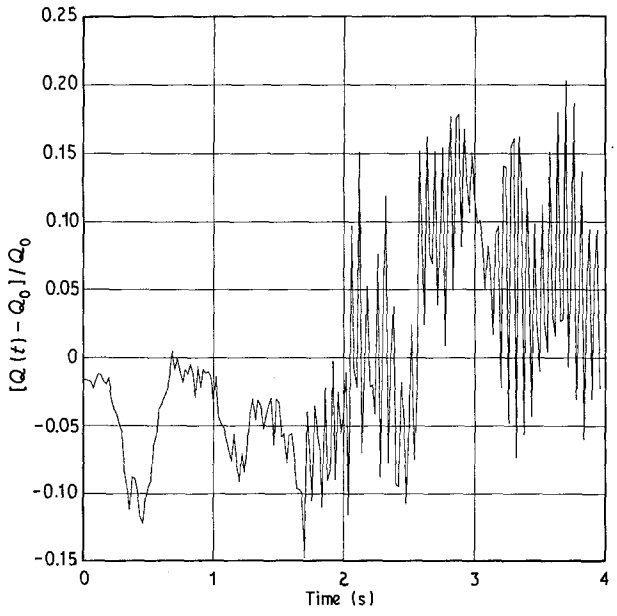

Figure 6 Time signal of oscillating sphere. Melting occurs at $t \approx 1.7$ s.

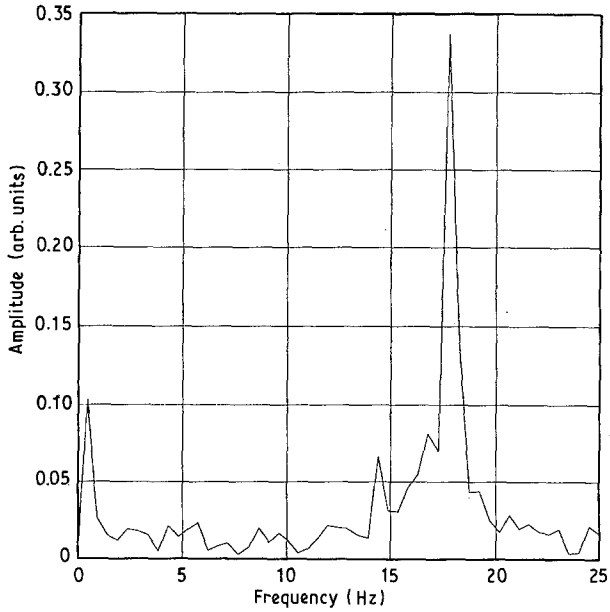

Figure 7 Fourier spectrum of oscillating sphere.

4.2. Viscosity measurements

From the experiment on the KC-135 flight, no viscosity data could be derived. This is due to several limiting factors. Firstly, the experimental apparatus and the environment on board the aircraft caused too many disturbances on the sample. Secondly, a strong d.c. magnetic field was used to damp the translational oscillations of the sample. This field, of course, also damped the surface oscillations drastically, thereby masking any damping due to viscosity. The magnetic damping can be estimated as [18]

$$\Gamma = \frac{\tilde{\sigma}B^2}{\rho} \tag{32}$$

where $\tilde{\sigma}$ is the electrical conductivity and ρ is the mass density. In order to measure viscosities, this must be much less than viscous damping (Equation 11): $\Gamma \ll \gamma$. For typical values, we obtain a tolerable magnetic field strength of $B \approx 1$ mT, whereas the KC-135 set-up had $B \approx 50$ mT.

Finally, the measuring time, $\Delta\tau = 2$ s, is too short to detect a damping constant $1/\gamma \approx 10$ s.

These problems will be eliminated in the proposed experiment for the IML-2 Spacelab-mission [8]. This investigation, scheduled for 1993, is intended to yield precise data on both surface tension and viscosity for a number of interesting metals.

Acknowledgements

A number of people participated at different stages and with different contributions to the results presented here. The experiment idea is the outcome of numerous discussions with B. Feuerbacher and J. Szekely. G. Lohöfer, J. Piller and R. Knauf performed the experiment on the KC-135 flight, and L. Persson did most of the image processing. K. Mills and the group at NPL provided the chemical analysis of the sample. D. Cummings and the Open University

made available their work on aspherical drops prior to publication. Sincere thanks are due to all of them.

References

1. D. STROUD and M. J. GRIMSON, *J. Non-Cryst. Solids* **68** (1984) 231.
2. B. C. ALLEN, in "Liquid Metals", edited by S. Z. Beer (Dekker, New York, 1972) p. 161.
3. B. J. KEENE, *Int. Mater. Rev.* **1** (1988) 1.
4. J. F. PADDAY, in "Surface and Colloid Science", edited by E. Matijevic (Wiley, New York, 1969).
5. R. SANGIORGI, G. CARACCIOLO and A. PASSERONE, *J. Mater. Sci.* **17** (1982) 2895.
6. R. WILLNECKER, D. M. HERLACH and B. FEUERBACHER, *Appl. Phys. Lett.* **49** (1986) 1339.
7. W. H. REID, *Q. Appl. Math.* **18** (1960) 86.
8. I. EGRY, B. FEUERBACHER, G. LOHÖFER and P. NEUHAUS, Proceedings of the VIIth European Symposium on Materials and Fluid Sciences in Microgravity, Oxford, UK, 10–15 September 1989, ESA SP-295 (1990) p. 257.
9. M. E. FRASER, W.-K. LU, A. E. HAMIELEC and R. MURARKA, *Metall. Trans.* **2** (1971) 817.
10. J. SCHADE, A. McLEAN and W. A. MILLER, in "Undercooled Alloy Phases", edited by E. W. Collins and C. C. Koch, Proceedings of the 115th Annual Meeting of TMS-AIME (1986) p. 233.
11. B. J. KEENE, K. C. MILLS, A. KASAMA, A. McLEAN and W. A. MILLER, *Metall. Trans.* **B17** (1986) 159.
12. L. LIGGIERI and A. PASSERONE, *High Temp. Technol.* **7** (1989) 82.
13. E. C. OKRESS, D. M. WROUGHTON, G. COMENETZ, P. H. BRACE and J. C. R. KELLY, *J. Appl. Phys.* **23** (1952) 545.
14. G. LOHÖFER, *SIAM J. Appl. Math.* **49** (1989) 567.
15. A. GAGNOUD, J. ETAY and M. GARNIER, *Trans. ISIJ* **28** (1988) 36.
16. D. L. CUMMINGS and D. A. BLACKBURN, *J. Fluid Mech.*, submitted.
17. A. V. OPPENHEIM and R. W. SCHAFER, "Digital Signal Processing" (Prentice Hall, Englewood Cliffs, NJ, 1975).
18. J. D. JACKSON, "Classical Electrodynamics" (Wiley, New York, 1962).

Received 9 April
and accepted 2 August 1990